AIX-MARSEILLE UNIVERSITY

DOCTORAL SCHOOL: Physics and Material Science

Submitted with the view of obtaining the degree of doctor

Discipline: Material Science
Specialty: Characterisation of porous materials

Paul A. Iacomi

Titre de la thèse: sous-titre de la thèse

Defended on JJ/MM/AAAA in front of the following jury:

Prénom NOM	Affiliation	Rapporteur
Prénom NOM	Affiliation	Rapporteur
Prénom NOM	Affiliation	Examinateur
Prénom NOM	Affiliation	Examinateur
Prénom NOM	Affiliation	Examinateur
Prénom NOM	Affiliation	Directeur de thèse

Abstract

Abstract is here.

Acknowledgements

Acknowledgements go here

Contents

Contents

2. Extending bulk analysis of porous compounds through calorimetry

2.1. Introduction

While the previous chapter focused on a physical description of adsorption and its use for the characterisation of porous materials, a rigorous thermodynamic background was omitted. However, an understanding of the energetic aspects of adsorption allows for one of the most powerful applications of adsorption methodology, namely a representation of the kinds of physical and chemical processes occurring during adsorption. Through a direct or indirect measurement of the so-called enthalpy of adsorption (h_{ads}), information about surface composition, the strength of adsorbate-guest and guest-guest interactions, phase change phenomena and, in some cases, transitions in the adsorbing material itself can be obtained.

Furthermore, the enthalpy of adsorption is a crucial parameter in an industrial setting. Owing to the exothermic nature of adsorption in combination with the strong influence of temperature on the performance of adsorbent materials, h_{ads} is often regarded as the most important parameter in the design of beds and columns, alongside working capacity and adsorption/catalytic selectivity. The enthalpy of adsorption is also a measure of the guest-host interactions, which have to be overcome for material regeneration. As such, it represents an important metric of the energy efficiency of the process.

As such the insight afforded through measurement of the energetic components of adsorption can prove invaluable for investigating subtle changes in adsorbent materials which lead to the kind of variability encountered in chapter 1. The thoroughness and suitability of the activation procedure, presence of surface functionalisations, defect formation such as inclusion of counterions and vacancies and activation-driven phenomena such as gate opening, state switching or flexibility all be qualitatively and, with careful methodology, even quantitatively analysed.

Chapter summary

First, an overview of the theoretical aspects underpinning the energetics of adsorption is presented. The methods section will go into detail in the available methodology for studying the enthalpy of adsorption on surfaces and in pores. The final part of the chapter will explore the use of combined adsorption and calorimetric measurements as a way of extending characterisation of porous materials.

Contributions

The isotherms on the Takeda 5A carbon were recorded by Andrew Wiersum during his thesis. The sample of Zr Fumarate MOF was synthesised in the group of Prof. Peter Behrens, from the University of Hannover, Germany. All measurements on this sample and data processing were performed by Paul Iacomi in the Madirel Laboratory, Marseille.

2.2. Energetics of adsorption

2.2.1. Forces involved in adsorption

From a classical molecular point of view, we can define the guest-host and guest-guest interactions as a sum of several components with distinct physical meaning.

$$\Phi_t = \Phi_R + \Phi_D + \Phi_C + \Phi_I \tag{2.1}$$

The first two types of interaction, namely short range electrostatic repulsion between the electron clouds of neighbouring atoms Φ_R and long range dispersion Φ_D arising from incidental short-lived partial charges are common to all atoms, and can therefore be called "non-specific". Such interactions are commonly modelled through the use of a Lennard-Jones type potential function.

$$V_{\mathrm{LJ}} = 4\varepsilon \left[\left(\frac{\sigma}{r} \right)^{12} - \left(\frac{\sigma}{r} \right)^{6} \right] \tag{2.2}$$

The latter two types, Coulombic interactions Φ_C and induction interactions Φ_R arise from permanent charges and multipoles in the system. Coulombic interactions are attraction and repulsion interactions between charges such as molecular ions, permanent dipoles and quadrupoles. Induction, also known as polarization or Debye forces, is the interaction between a charged particle or a multipole with the induced multipole in a non-charged system. The ease of inducing such an interaction in a molecule is termed polarizability. These interactions can be referred to as "specific".

Therefore, in the standard definition of adsorption, only Van-der-Waals forces are responsible. However, depending on the systems involved, stronger interactions such as hydrogen bonding, electron sharing, stacking or π interactions may also play a role in the overall stability of the guest-host attraction.

The total interactions can also be broken down as contributions from guest-host interactions and guest-guest interactions. If changes in the adsorbent occur as a result of adsorption, a host-host or self-potential interaction should be considered. The guest-host interaction can be assumed constant for a homogeneous surface or a function of coverage, in the case of a heterogeneous surface.

2.2.2. Adsorption thermodynamics

As mentioned in the previous section, adsorption is a consequence of intermolecular attraction between the material surface and the molecules of the fluid. The sum of all interactions accounts for the depth of the potential well and therefore for the energy corresponding to the process. As this energy is net positive, adsorption is an overall exothermic phenomenon.

However, in order to make the transition from a molecular viewpoint to a macroscale bulk fluid representation of adsorption, the a thermodynamic description of the adsorbed phase of the process must be performed.

The Gibbs surface excess approach

A description of the adsorbed phase can be made through expressing the change in density or concentration of fluid from the adsorbent surface to the bulk phase. The density has a maxima in the immediate zone close to the surface, and then decreases until it reaches the density of the bulk fluid. However, when defined as such, the boundary between the two phases is difficult to pinpoint. Therefore, in most cases it is useful to employ the concept of the Gibbs dividing surface.
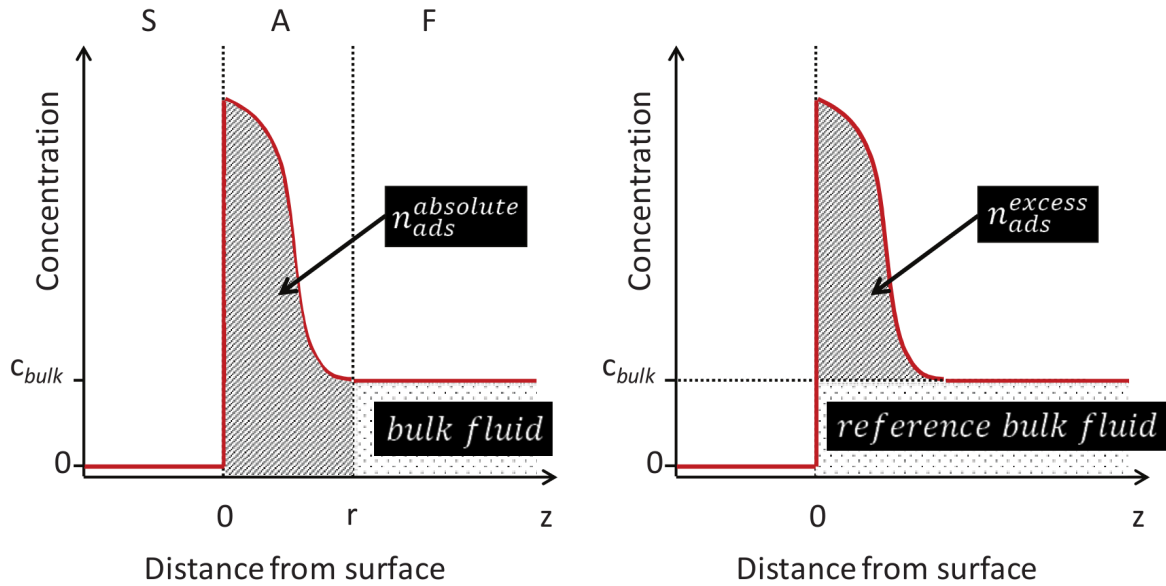
Figure 2.1.: Representation of the adsorbed and bulk phases according to the (left) layer model and the (right) Gibbs dividing surface approach. Adapted from Rouquerol et al..[1]

This approach describes the adsorbed phase only in terms of an *excess* from the properties of the bulk phase. As represented in Figure 2.1, the total amount adsorbed

can be defined as:

$$n^a_{ads} = A \int_0^r c \, dz \tag{2.3}$$

The imaginary Gibbs dividing surface is usually placed parallel to the real surface of the adsorbent and in the resulting system, the concentration of the adsorbent in the adsorbed phase are expressed as an excess from the concentration of the bulk fluid. The relationship between the total amount adsorbed and the excess amount adsorbed is then:

$$n^\sigma_{ads} = n^a_{ads} + V_{ads} \cdot c_{bulk} \tag{2.4}$$

As long as the volume of the adsorbed layer V_{ads} can be considered negligible and the concentration of adsorbate in the bulk phase c_{bulk} is low, the total amount adsorbed and the surface excess amount may be considered as approximately equal. This is usually the case for experiments such as nitrogen adsorption at $77\,\mathrm{K}$, or room temperature adsorption below $1\,\mathrm{bar}$. At high pressures or when the difference in concentration between the adsorbed and the bulk phase is low, the total amount adsorbed begins to diverge significantly from the surface excess.

Without corrections, both the gravimetric and manometric method of adsorption will measure excess amounts adsorbed. In the case of adsorption in porous materials, the volume of the adsorbed phase may be taken as total pore volume.

Differential enthalpy of adsorption

Adsorption can be considered as a closed system of constant volume V and temperature T. No mass of material crosses the system boundary, therefore the total change in chemical potential is also zero $d\mu = 0$. Through a derivation[1] of the gas and adsorbed phase/adsorbent energies we may obtain a Gibbs-Duhem type equation:

$$d\mu^\sigma = -\frac{S^\sigma}{n^\sigma} dT + \frac{A}{n^\sigma} d\pi \tag{2.5}$$

from which the Gibbs adsorption isotherm (Equation 1.1) may be derived, as well as

$$\ln p = \frac{\dot{u}^\sigma_{T,\Gamma} - u^g_T - RT}{RT} - \frac{\dot{s}^\sigma_{T,\Gamma} - s^g_0}{R} = \frac{\Delta_{ads}\dot{h}_{T,\Gamma}}{RT} - \frac{\Delta_{ads}\dot{s}_{T,\Gamma}}{R} \tag{2.6}$$

an expression relating the differential enthalpy of adsorption $\Delta_{ads}\dot{h}_{T,\Gamma}$ and the differential entropy of adsorption $\Delta_{ads}\dot{s}_{T,\Gamma}$ to the pressure of an ideal gas. The relationship between the differential enthalpy and the differential energy of the adsorbed phase is given by:

$$\Delta_{ads}\dot{h}_{T,\Gamma} = \Delta_{ads}\dot{u}_{T,\Gamma} - RT \tag{2.7}$$

Application of differential enthalpy of adsorption to the characterisation of materials

As the differential enthalpy of adsorption is a measure of the interaction taking place during adsorption, it is often used in conjunction with the isotherm to study the properties of adsorbent materials. Unfortunately, only the total sum of individual interactions is measurable through direct methods. Therefore, the absolute contribution of each component presented in subsection 2.2.1 cannot be determined. However, with careful choice of experiments and interpretation of results, specific factors may be compared.

When adsorbing in microporous materials, the filling of the different types of pores may be followed, as the confinement energy for each pore is specific to its size, assuming identical surface composition. Effect of the material structure and surface chemistry on guest-host interactions can be gauged through alteration of a single property. For example through changing the Si/Al ratio in a series of MFI zeolites[2], the impact of the adsorbent on the initial adsorption behaviour may be studied. Other examples include the role of compensation cations in an ion-exchanged X-faujasite[3,4] or the influence of open metal sites[5] and their distribution.[6] The contribution of non-specific effects such as π backbonding in porous coordination compounds[7] can be examined by the choice of a suitable probe pair, such as a saturated and unsaturated version of a hydrocarbon (ethane/ethylene/acetylene). Guest-guest interactions during adsorption may also be monitored with cooperative effects such as 2-dimensional analogues of phase changes[8] visible as peaks in the enthalpy curve. If the adsorbate itself undergoes structural deformation during adsorption, as is the case in soft materials, the measured enthalpy of adsorption can be a clear indication of such changes.[9] The net enthalpy of adsorption is such a system is often lowered through the energetic contribution of the state change of the adsorbate, and may be of use for a reduction in the thermal load to be dissipated for adsorption or required to recover the adsorbed material.[10]

The differential enthalpy of adsorption is often represented as a function of partial coverage. In Figure 2.2, isotherm types as defined by IUPAC[11] are presented together with a typical differential enthalpy curve.[12] Type I isotherms often have an initial plateau, corresponding to adsorption in micropores until a sharp decrease at complete pore filling occurs. If the surface of the pores is heterogeneous, higher energy sites will be occupied first, resulting in a sharp slope at low loadings. Multilayer adsorption in non-porous or mesoporous materials (II and IV) yields a slowly decreasing enthalpy curve, as the solid-guest interactions drop off with increasing layers adsorbed. Finally, cooperative adsorption on non-interacting surfaces (such as water adsorption in hydrophobic porous materials) as seen in a type III isotherm, often gives rise to initial enthalpies of adsorption which are below the enthalpy of vaporisation. Finally, distinct peaks often accompany multilayer adsorption (Type VI) which are an indication of epitaxial phase changes at completion of each layer.[2,8,13]
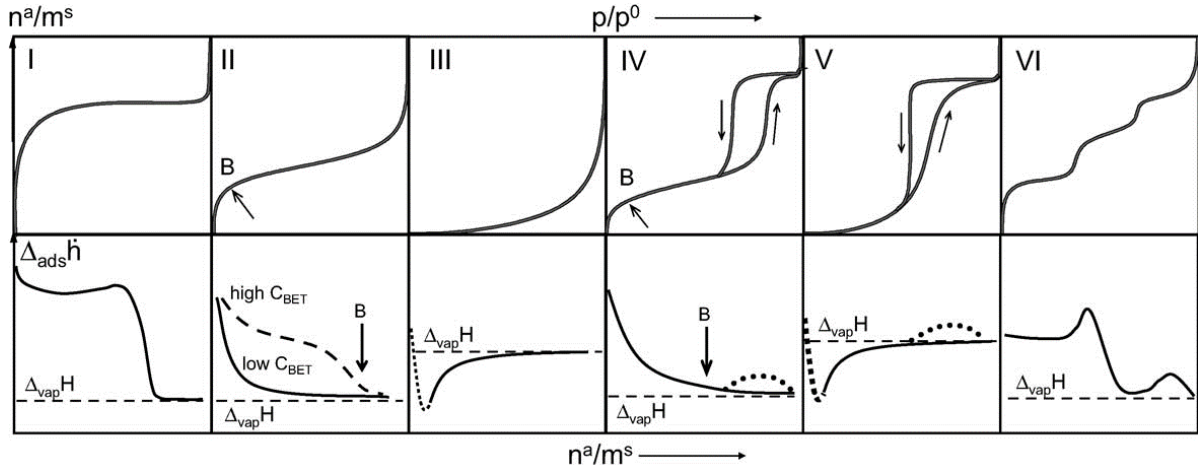
Figure 2.2.: Generalized curves of differential enthalpy of adsorption with respect to coverage corresponding to different IUPAC-defined isotherm types. Adapted from Llewellyn and Maurin. [12]

2.3. Measuring the enthalpy of adsorption

Experimentally, two methods are widely used for determining the enthalpy of adsorption. The first relies on measurement of two or more isotherms at different temperatures and the use of a Clausius-Clapeyron-type equation for indirect calculation, while the second is a direct measurement of the evolved heat during adsorption using calorimetry.

A value for the enthalpy of adsorption in a particular system may also be obtained from computer simulation methods. The accuracy of these procedures depends on the accuracy of the chosen model of interaction between simulated molecules.

2.3.1. Isosteric enthalpy of adsorption

If the differential enthalpy of adsorption is assumed be independent of temperature, Equation 2.6 can be differentiated with respect to temperature keeping the surface adsorbed amount constant to obtain an equation analogous to the Clausius-Clapeyron equation:

$$\left(\frac{\partial \ln p}{\partial T}\right)_{n_a} = -\frac{\Delta_{ads}\dot{h}_{T,\Gamma}}{RT^2} \tag{2.8}$$

The equation can be rearranged to calculate the differential enthalpy:

$$\Delta_{ads}\dot{h}_{T,\Gamma} = R\left(\frac{\partial \ln p}{\partial 1/T}\right)_{\Gamma} \tag{2.9}$$

where $\Delta_{ads}\dot{h}_{T,\Gamma}$ is the often termed the isosteric enthalpy of adsorption.

In order to approximate the partial differential, two or more isotherms are measured at different temperatures. Afterwards the isosteric enthalpy of adsorption can be calculated

by using the pressures at which the loading is identical using the rearranged equation. By plotting the values of $\ln p$ against $1/T$ we should obtain a straight line with a slope of $-\Delta_{ads}\dot{h}_{T,\Gamma}/R$.

As experimental isotherms do not necessarily have points spaced at equal loading intervals, interpolation is usually used to obtain data at the desired points. Alternatively, a model may be used to first fit the isotherm, which is then used for the calculation.

The isosteric enthalpy is sensitive to differences in pressure between the two isotherms. If the isotherms measured are too close together, the error margin will increase. The method also assumes that isosteric enthalpy does not vary with temperature. If the variation is large for the system in question, the calculation will lead to unrealistic values. The isosteric method is less suited if applied to soft materials, where the structural changes are often temperature dependent themselves.

Even with carefully measured experimental data, there are two assumptions used in deriving Equation 2.9: an ideal bulk gas phase and a negligible adsorbed phase molar volume. These have a significant effect on the calculated isosteric enthalpy of adsorption, especially at high relative pressures and for heavy adsorbates.

Measurements in this work

2.3.2. Microcalorimetry

A direct measurement of the enthalpy of adsorption is possible using calorimetric methods. An isothermal calorimeter is most often used for this purpose, to best approximate a reversible exchange of heat between the system under investigation and the surrounding heat sink. To allow for a complete integration of evolved heat, with minimal losses, a 3D Tian-Calvet thermopile [14] can be used. In order to cancel out variations in environment, differential mounting is employed, in which the signal is the difference in voltage between a reference and experimental thermopile. In order to ensure the "isothermicity" of the calorimeter, a suitable heat sink must be used, leading to two types of design. Ambient temperature calorimeters use resistance heating to maintain the internal temperature, while utilising the environment as its heat sink. At low temperature, the environment acts as a heat source and therefore the heat sink must be provided, often in the form of a constant-temperature bath undergoing a phase change or through a cryostat. Sketches of an ambient and a low temperature differential Tian-Calvet calorimeter can be seen in Figure 2.3.

Care must be taken to ensure that the recorded heat through such an experiment can be related directly to adsorption enthalpy and not to other heat effects. The adsorbate and gas residing inside a calorimeter is best represented by an open system, where the introduction of adsorbate is done through steps that are small enough to consider a reversible process. [15] The accepted convention is that the adsorbate itself is inert and therefore does not contribute to the variation of any state function. In these conditions, the change in internal energy of the adsorbate can be written as:

$$dU = dQ_{rev} + dW_{rev} + u_T^g dn \tag{2.10}$$

(a) Ambient-temperature calorimeter   (b) Low-temperature calorimeter
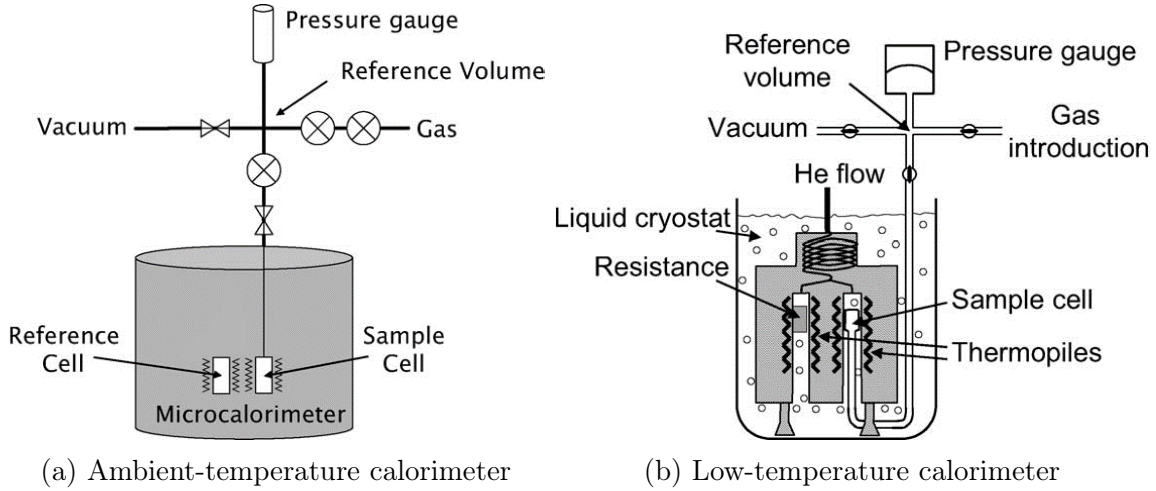
Figure 2.3.: Two types of isothermal Tian-Calvet calorimeters for adsorption measurements, specialized for different temperature ranges. Adapted from Llewellyn and Maurin.[12]

where dQ_{rev} is the reversibly exchanged heat which is measured by the calorimeter. dW_{rev} is the reversible work done by the gas against the external pressure. In the cell volume measured by the calorimeter (V_C), this work may be expressed as

$$dW_{rev} = RT dn^\sigma + V_C dp \qquad (2.11)$$

If the previous two equations are combined and differentiated with respect to the amount adsorbed n^σ, then we obtain the equation for the differential heat of adsorption.

$$\frac{dQ_{rev}}{dn^\sigma} + V_C \frac{dp}{dn^\sigma} = \frac{dU^\sigma}{dn^\sigma} - u^g - RT = \Delta_{ads}\dot{h}_{T,\Gamma} \qquad (2.12)$$

Two options exist regarding the method of introduction of adsorbate: the continuous and the discontinuous or point-by-point method. In the point-by-point method, discrete insertion steps are made. A reference volume is filled with gas at a pressure p, which is allowed to equilibrate before a valve between the reference volume and the cell containing the adsorbate is opened, letting the gas adsorb onto the material. With small enough steps, the assumption of a reversible system can be approximated. The peak in the calorimetric signal is integrated over time to give the total energy released during this adsorption step.

In the other method, the flow of adsorbate is continuous, usually kept constant by a restriction in the pipe diameter which is severe enough to allow the gas to enter sonic flow regimes. At this point, the flowrate is no longer influenced by a pressure differential, instead becoming a function only of upstream pressure and environment temperature. The heat evolved during adsorption (or required during desorption) is therefore measured either as discrete peaks, corresponding to each introduction event or as a continuous heat curve. An example of such a signal for each method presented in Figure 2.4.

51

(a)   (b)

Figure 2.4.: Typical pressure and calorimeter signals for the two available methods of introducing adsorbate into the measurement cell (a) discontinuous and (b) continuous.
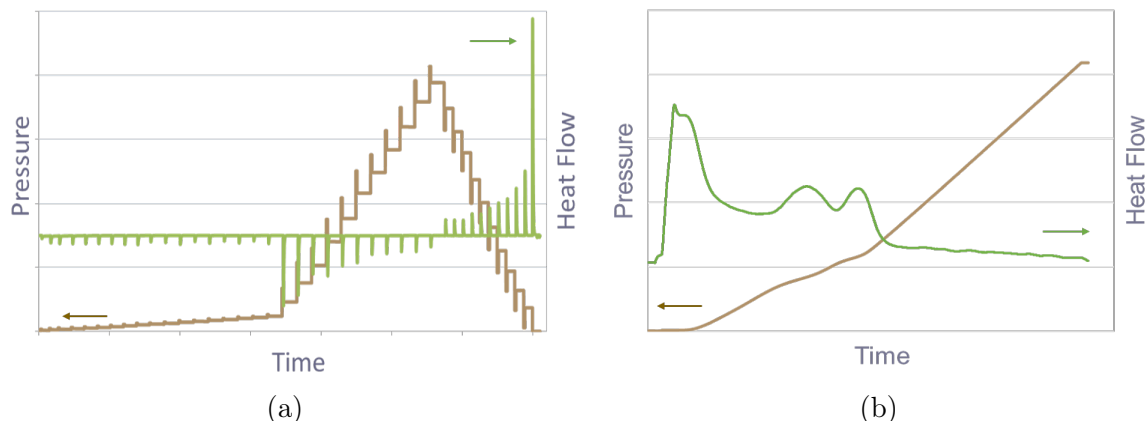
The point-by-point method is less accurate than a continuous introduction, as the measured heat is necessarily a cumulative value of instantaneous differential enthalpy for the coverage range of each adsorbed point. However, it has the advantage of ensuring complete equilibrium at each step, by observing the return to the baseline of the calorimetry signal or a stable pressure signal. On the other hand, the continuous method allows for subtle changes in the differential enthalpy of adsorption, such as those corresponding to adsorbed phase changes, to be seen experimentally. Additionally, the time-resolved data can be used to investigate transient phenomena. Equilibrium between the adsorbed phase and gas phase is no longer guaranteed, and must be tested for by performing multiple experiments at different adsorbate flowrates. Alternatively, the experiment can be stopped to observe that the time for the heat signal to return to its baseline does not diverge from the dead time of the calorimeter.

Measurements in this work

In this thesis, combined isotherms and enthalpy of adsorption measurements were made experimentally using a Tian-Calvet type microcalorimeter coupled with a home-made manometric gas dosing system.[12] Two calorimeter designs were used, one for ambient temperature and one for low temperature adsorption, as displayed in Figure 2.3.

The method of adsorbate introduction can be chosen either as continuous or discontinuous. For routine measurements, the point-by-point method is preferred, as it is guaranteed to achieve equilibrium between the material and the adsorbate removing the influence of diffusion effects. For each injection of gas, equilibrium was assumed to have been reached after 90 min to 150 min depending on the sample and adsorbate used. This was confirmed by the return of the calorimetric signal to its baseline ($<5\,\mu$W).

At low coverage the error in the signal can be estimated to around $\pm\ 0.2\,\mathrm{kJ\,mol^{-1}}$. Between 50 mg to 200 mg of sample is used in each experiment, such that the specific surface area inside the calorimeter cell is larger than $50\,\mathrm{m^2/g}$. A complete error analysis

for the resulting isotherms and enthalpy curves can be found in **??**.

Data processing

2.4. Measurements and analysis

2.4.1. Comparison between the enthalpy of adsorption measured through the direct and indirect method

In order to view the difference that may arise between the isosteric and calorimetric method of measuring the enthalpy of adsorption, a sample of UiO-66(Zr) previously used for a study of carbon dioxide[16] adsorption was also measured through microcalorimetry. Two previous isotherms were recorded at 303 K and 323 K respectively, with the new isotherm measured in the calorimeter at 303 K. The complete set of isotherms is loaded into `pyGAPS` and plotted by the pygaps.plot_iso() function as seen in Figure 2.5a. To calculate the isosteric enthalpy of adsorption, the two isotherms measured for this purpose are first fitted with a virial type model, then passed through the pygaps.isosteric_heat() function. Results from the calculation are overlaid on top of the measured calorimetric data in Figure 2.5b as a function of amount adsorbed.

(a)   (b)
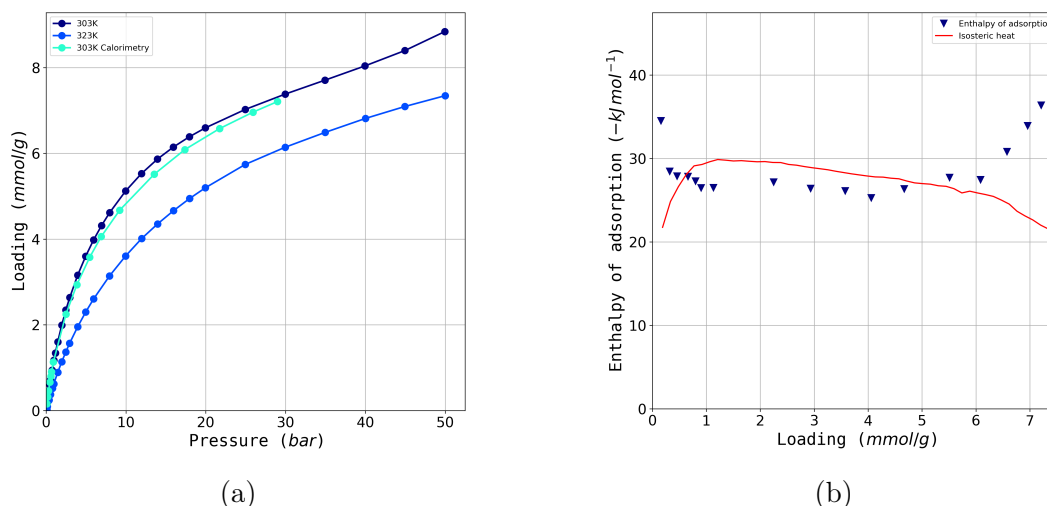
Figure 2.5.: Calculation of enthalpy of adsorption: (a) the dataset of isotherms used and (b) the calculated isosteric heat (red line) together with the measured differential enthalpy of adsorption (blue triangles)

The two datasets overlap for the most part but diverge at low loadings and near complete coverage. At low loading the small errors in pressure measurement introduce large errors in the isosteric enthalpy. This, together with the breakdown of the assumption of equilibrium due to active sites in the MOF mean that the calorimetric measurement is more suited to this range. At higher loadings, where the isotherm reaches a plateau

and the change in adsorbed amount is small between each adsorbate insertion, errors are introduced in the direct calculation of the enthalpy of adsorption. Here, the indirect calculation provides the more accurate results. As such, the two techniques are complementary.

2.4.2. Analysis of a carbon sample for gas separation applications

A sample of reference carbon Takeda 5A (section B.1) is to be investigated for an in-depth characterisation of the adsorption behaviour of pure gases, with a focus on describing the pore environment. Afterwards, the performance of different binary separations is evaluated, such as CO_2/N_2 and propane/propylene.

Pure gas adsorption data has been recorded at 303 K in conjunction with microcalorimetry on N_2, CO, CO_2, CH_4, C_2H_6, C_3H_6 and C_3H_8. The complete dataset is plotted with the pygaps.plot_iso() function and can be seen in Figure 2.6a.

Nitrogen and carbon monoxide are similar in their adsorption behaviour, with a nearly linear isotherm and low capacities. Hydrocarbons are adsorbed with higher loadings, with both propane and propylene reaching a plateau at low pressures. Propylene is seen to have a higher capacity than propane, with packing effects as a likely cause. Carbon dioxide has the highest loading capacity of the entire dataset.

Two parameters can be useful in characterising the local pore environment before guest-guest interactions come into effect: the Henry constant at low loadings as well as the initial enthalpy of adsorption. Both can be calculated with `pyGAPS`, with several options in regard to the methodology. Here, Henry's constant is calculated using the pygaps.initial_henry_virial() function, which fits a virial model to the isotherm and then takes the limit at loading approaching zero. The initial enthalpy of adsorption is obtained through the pygaps.initial_enthalpy_comp() function. This fits the enthalpy curve to a compound contribution from guest-host interaction, defects, guest-guest attraction and repulsion using a minimization algorithm. The results of the calculations are plotted versus the polarizability of the gas used, which can be obtained from the respective `Adsorbate` class. Figure 2.6b shows that both the parameters fall on a linear trend, which suggests that the interactions between those guests and the pore walls are mostly due to Lennard-Jones interactions. Carbon dioxide has a higher enthalpy of adsorption than the baseline due to the contribution from its quadrupole moment. There is almost a complete overlap between propane and propylene, which leads to the conclusion that the unsaturated double bond does not interact in a specific way with the carbon surface. The difference between the two isotherms is due exclusively to steric and packing effects.

Figure 2.6.: Takeda 5A dataset processing: (a) the experimental dataset all recorded gases and (b) the calculated trends of initial heat of adsorption and Henry's constant

2.4.3. Discovering possible separations

Material

Zr Fumarate, also known as MOF-801, is a fumaric acid analogue of the well-known UiO-66(Zr) framework.[17] Its structure is similar to that of UiO-66, although the smaller non-linear linker leads to a lowering of symmetry and a slight tilting in the Zr-O clusters, as depicted in Figure 2.7. The MOF is synthesised using the modulated synthesis method and formic acid as the modulator to increase the crystalinity of the material. Indeed, when not using this approach, the resulting material is nearly amorphous.[18] In this study the sample was synthesised according to the procedure detailed in section B.3.
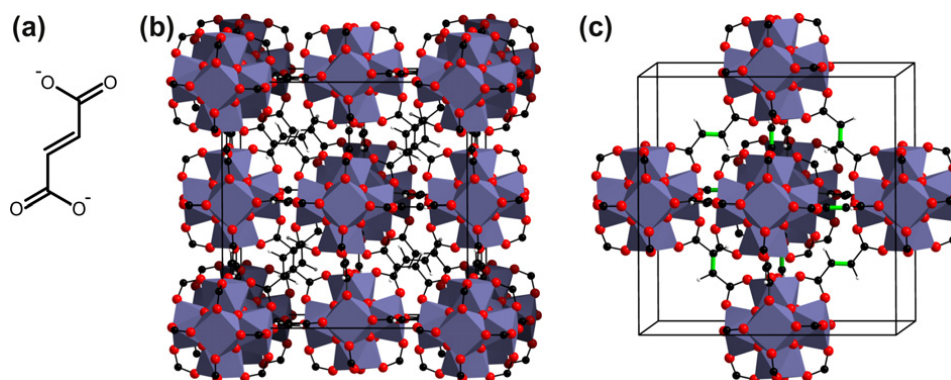
Figure 2.7.: (a) The fumarate linker used in the Zr Fumarate MOF, an ionic form of *trans*-butenedioic acid and (b) and (c) the structural model of the MOF. Illustration adapted from Wißmann et al..[17]

Zr Fumarate has recently been the subject of interest due to its high water stability[19],

as well as its potential to be synthesised through green synthesis routes[20] or direct monolith formation with a gel approach.[21]

Furthermore, the material has a remarkably steep water adsorption behaviour at low pressure[22], which has led to its possible application as a water scavenger membrane[23] or in a water harvesting device which would capture water from air in low relative humidity environments such as the desert. While initial attempts[24] were criticised for overpromising performance, more recent modifications to such a system have addressed some of these concerns.[25]

The low relative pressure of water adsorption has highlighted the contribution of defects[26] in shifting the adsorption isotherm, an effect arising from cooperative interactions and initial clustering of water molecules on defect sites.[27]

As the properties of the MOF diverge from the ideal properties indicated by the structure, an experimental study to test for the adsorption or separation of other molecules may reveal unexpected applications.

Results

Adsorption isotherms of nine probe gasses were recorded at 303 K through combined manometry and microcalorimetry as described in subsection 2.3.2. The complete dataset can be seen in Figure 2.8a.

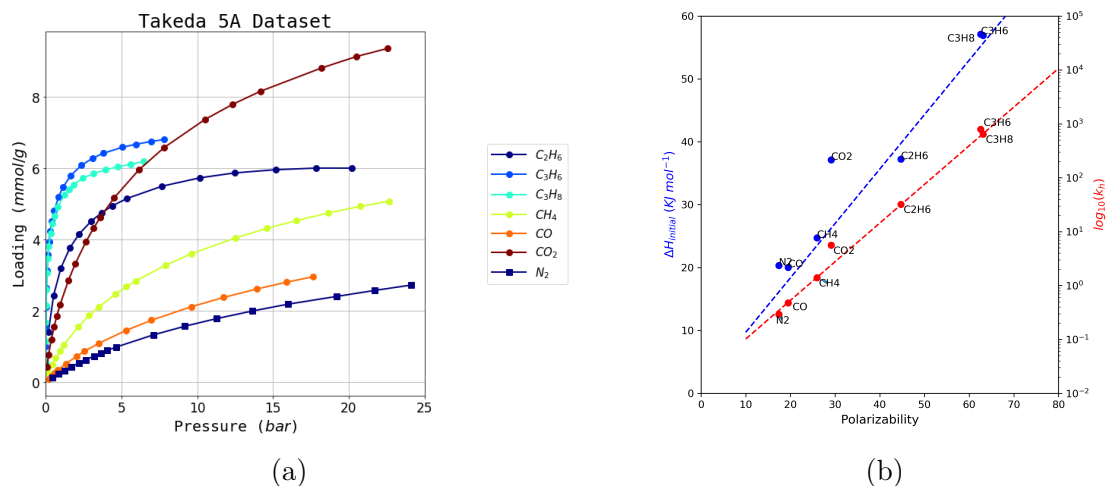(a)   (b)
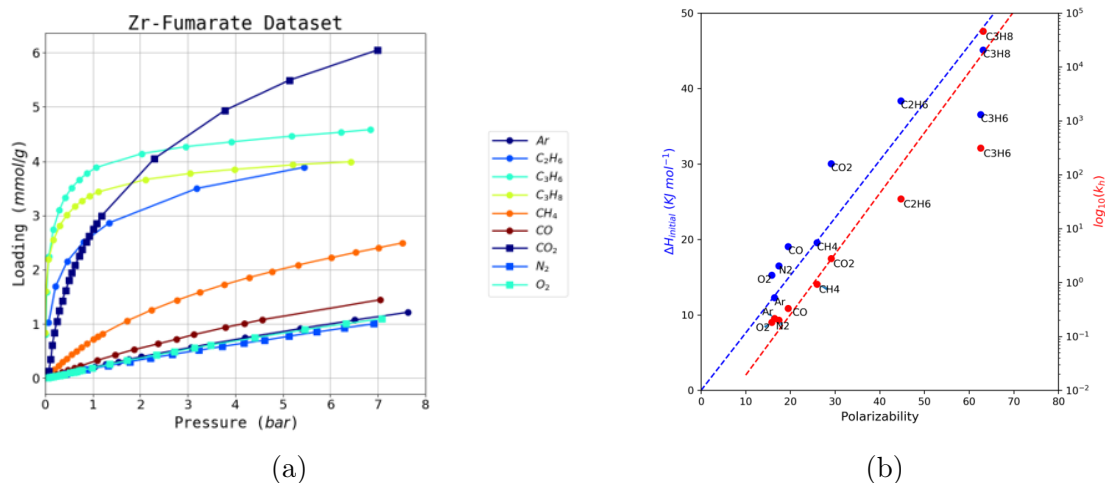
Figure 2.8.: (a) The experimental dataset all recorded gases and (b) the calculated trends of initial heat of adsorption (red) and Henry's constant (blue). The dotted lines are best fit lines to the series of unsaturated hydrocarbons.

Values for initial Henry's constant and initial enthalpy of adsorption were calculated using the methods available in pyGAPS. The same trend as with the Takeda 5A sample was plotted in Figure 2.8b.

2.5. Conclusion

Bibliography

[1] Jean Rouquerol, Françoise Rouquerol, Philip L. Llewellyn, Guillaume Maurin, and Kenneth Sing. *Adsorption by Powders and Porous Solids : Principles, Methodology and Applications.* 2013. ISBN 978-0-08-097035-6.

[2] P. L. Llewellyn, J. P. Coulomb, Y. Grillet, J. Patarin, H. Lauter, H. Reichert, and J. Rouquerol. Adsorption by MFI-type zeolites examined by isothermal microcalorimetry and neutron diffraction. 1. Argon, krypton, and methane. *Langmuir*, 9(7):1846–1851, July 1993. ISSN 0743-7463, 1520-5827. doi: 10.1021/la00031a036.

[3] G. Maurin, P.L. Llewellyn, Th. Poyet, and B. Kuchta. Adsorption of argon and nitrogen in X-faujasites: Relationships for understanding the interactions with monovalent and divalent cations. *Microporous and Mesoporous Materials*, 79(1-3):53–59, April 2005. ISSN 13871811. doi: 10.1016/j.micromeso.2004.10.017.

[4] G. Maurin, Ph. Llewellyn, Th. Poyet, and B. Kuchta. Influence of Extra-Framework Cations on the Adsorption Properties of X-Faujasite Systems: Microcalorimetry and Molecular Simulations. *The Journal of Physical Chemistry B*, 109(1):125–129, January 2005. ISSN 1520-6106, 1520-5207. doi: 10.1021/jp0461753.

[5] Lukáš Grajciar, Andrew D. Wiersum, Philip L. Llewellyn, Jong-San Chang, and Petr Nachtigall. Understanding CO 2 Adsorption in CuBTC MOF: Comparing Combined DFT–ab Initio Calculations with Microcalorimetry Experiments. *The Journal of Physical Chemistry C*, 115(36):17925–17933, September 2011. ISSN 1932-7447. doi: 10.1021/jp206002d.

[6] Ji Woong Yoon, You-Kyong Seo, Young Kyu Hwang, Jong-San Chang, Hervé Leclerc, Stefan Wuttke, Philippe Bazin, Alexandre Vimont, Marco Daturi, Emily Bloch, Philip L. Llewellyn, Christian Serre, Patricia Horcajada, Jean-Marc Grenèche, Alirio E. Rodrigues, and Gérard Férey. Controlled Reducibility of a Metal-Organic Framework with Coordinatively Unsaturated Sites for Preferential Gas Sorption. *Angewandte Chemie International Edition*, 49(34):5949–5952, August 2010. ISSN 14337851. doi: 10.1002/anie.201001230.

[7] Miroslav Rubeš, Andrew D. Wiersum, Philip L. Llewellyn, Lukáš Grajciar, Ota Bludský, Petr Nachtigall, Miroslav Rubes, Andrew D. Wiersum, Philip L. Llewellyn, Lukáš Grajciar, Ota Bludský, and Petr Nachtigall. Adsorption of propane and propylene on CuBTC metal-organic framework: Combined theoretical and experimental investigation. *Journal of Physical Chemistry C*, 117(21):11159–11167, May 2013. ISSN 19327447. doi: 10.1021/jp401600v.

[8] Jean Rouquerol, Stanislas Partyka, and Françoise Rouquerol. Calorimetric evidence for a bidimensional phase change in the monolayer of nitrogen or argon adsorbed on graphite at 77 K. *Journal of the Chemical Society, Faraday Transactions 1: Physical Chemistry in Condensed Phases*, 73:306, 1977. ISSN 0300-9599. doi: 10.1039/f19777300306.

[9] Sandrine Bourrelly, Philip L. Llewellyn, Christian Serre, Franck Millange, Thierry Loiseau, and Gérard Férey. Different Adsorption Behaviors of Methane and Carbon Dioxide in the Isotypic Nanoporous Metal Terephthalates MIL-53 and MIL-47. *Journal of the American Chemical Society*, 127(39):13519–13521, October 2005. ISSN 0002-7863. doi: 10.1021/ja054668v.

[10] Jarad A. Mason, Julia Oktawiec, Mercedes K. Taylor, Matthew R. Hudson, Julien Rodriguez, Jonathan E. Bachman, Miguel I. Gonzalez, Antonio Cervellino, Antonietta Guagliardi, Craig M. Brown, Philip L. Llewellyn, Norberto Masciocchi, and Jeffrey R. Long. Methane storage in flexible metal–organic frameworks with intrinsic thermal management. *Nature*, 527(7578):357–361, October 2015. ISSN 0028-0836, 1476-4687. doi: 10.1038/nature15732.

[11] Matthias Thommes, Katsumi Kaneko, Alexander V. Neimark, James P. Olivier, Francisco Rodriguez-Reinoso, Jean Rouquerol, and Kenneth S W Sing. Physisorption of gases, with special reference to the evaluation of surface area and pore size distribution (IUPAC Technical Report). *Pure and Applied Chemistry*, 87(9-10): 1051–1069, 2015. ISSN 13653075. doi: 10.1515/pac-2014-1117.

[12] Philip L. Llewellyn and Guillaume Maurin. Gas adsorption microcalorimetry and modelling to characterise zeolites and related materials. *Comptes Rendus Chimie*, 8(3-4):283–302, March 2005. ISSN 16310748. doi: 10.1016/j.crci.2004.11.004.

[13] P. L. Llewellyn, J. P. Coulomb, Y. Grillet, J. Patarin, G. Andre, and J. Rouquerol. Adsorption by MFI-type zeolites examined by isothermal microcalorimetry and neutron diffraction. 2. Nitrogen and carbon monoxide. *Langmuir*, 9(7):1852–1856, July 1993. ISSN 0743-7463, 1520-5827. doi: 10.1021/la00031a037.

[14] E Calvet and H Prat. *Recent Progress in Microcalorimetry*. 1963. OCLC: 893676446.

[15] Françoise Rouquerol, Jean Rouquerol, and Douglas H. Everett. Gas—solid interactions. General derivation of reaction enthalpies from the data of isothermal microcalorimetry. *Thermochimica Acta*, 41(3):311–322, November 1980. ISSN 00406031. doi: 10.1016/0040-6031(80)87207-8.

[16] Andrew D. Wiersum, Estelle Soubeyrand-Lenoir, Qingyuan Yang, Beatrice Moulin, Vincent Guillerm, Mouna Ben Yahia, Sandrine Bourrelly, Alexandre Vimont, Stuart Miller, Christelle Vagner, Marco Daturi, Guillaume Clet, Christian Serre, Guillaume Maurin, and Philip L. Llewellyn. An Evaluation of UiO-66 for Gas-Based Applications. *Chemistry - An Asian Journal*, 6(12):3270–3280, December 2011. ISSN 18614728. doi: 10.1002/asia.201100201.

[17] Gesa Wißmann, Andreas Schaate, Sebastian Lilienthal, Imke Bremer, Andreas M. Schneider, and Peter Behrens. Modulated synthesis of Zr-fumarate MOF. *Microporous and Mesoporous Materials*, 152:64–70, April 2012. ISSN 13871811. doi: 10.1016/j.micromeso.2011.12.010.

[18] Gesa Zahn, Philip Zerner, Jann Lippke, Fabian L. Kempf, Sebastian Lilienthal, Christian A. Schröder, Andreas M. Schneider, and Peter Behrens. Insight into the mechanism of modulated syntheses: *In Situ* synchrotron diffraction studies on the formation of Zr-fumarate MOF. *CrystEngComm*, 16(39):9198–9207, 2014. ISSN 1466-8033. doi: 10.1039/C4CE01095G.

[19] Gesa Zahn, Hendrik Albert Schulze, Jann Lippke, Sandra König, Uta Sazama, Michael Fröba, and Peter Behrens. A water-born Zr-based porous coordination polymer: Modulated synthesis of Zr-fumarate MOF. *Microporous and Mesoporous Materials*, 203:186–194, February 2015. ISSN 13871811. doi: 10.1016/j.micromeso. 2014.10.034.

[20] Helge Reinsch, Steve Waitschat, Sachin M. Chavan, Karl Petter Lillerud, and Norbert Stock. A Facile "Green" Route for Scalable Batch Production and Continuous Synthesis of Zirconium MOFs: A Facile "Green" Route for Scalable Batch Production and Continuous Synthesis of Zirconium MOFs. *European Journal of Inorganic Chemistry*, 2016(27):4490–4498, September 2016. ISSN 14341948. doi: 10.1002/ejic.201600295.

[21] Bart Bueken, Niels Van Velthoven, Tom Willhammar, Timothée Stassin, Ivo Stassen, David A. Keen, Gino V. Baron, Joeri F. M. Denayer, Rob Ameloot, Sara Bals, Dirk De Vos, and Thomas D. Bennett. Gel-based morphological design of zirconium metal–organic frameworks. *Chemical Science*, 8(5):3939–3948, 2017. ISSN 2041-6520, 2041-6539. doi: 10.1039/C6SC05602D.

[22] Hiroyasu Furukawa, Felipe Gándara, Yue-Biao Zhang, Juncong Jiang, Wendy L. Queen, Matthew R. Hudson, and Omar M. Yaghi. Water Adsorption in Porous Metal–Organic Frameworks and Related Materials. *Journal of the American Chemical Society*, 136(11):4369–4381, 2014. ISSN 0002-7863. doi: 10.1021/ja500330a.

[23] Youn Jue Bae, Eun Seon Cho, Fen Qiu, Daniel T. Sun, Teresa E. Williams, Jeffrey J. Urban, and Wendy L. Queen. Transparent Metal–Organic Framework/Polymer Mixed Matrix Membranes as Water Vapor Barriers. *ACS Applied Materials & Interfaces*, 8(16):10098–10103, April 2016. ISSN 1944-8244, 1944-8252. doi: 10. 1021/acsami.6b01299.

[24] Hyunho Kim, Sungwoo Yang, Sameer R Rao, Shankar Narayanan, Eugene A Kapustin, Hiroyasu Furukawa, Ari S Umans, Omar M Yaghi, and Evelyn N Wang. Water harvesting from air with metal-organic frameworks powered by natural sunlight. *Science*, 356(6336):430–434, April 2017. ISSN 0036-8075. doi: 10.1126/science.aam8743.

[25] Hyunho Kim, Sameer R. Rao, Eugene A. Kapustin, Lin Zhao, Sungwoo Yang, Omar M. Yaghi, and Evelyn N. Wang. Adsorption-based atmospheric water harvesting device for arid climates. *Nature Communications*, 9(1), December 2018. ISSN 2041-1723. doi: 10.1038/s41467-018-03162-7.

[26] Jongwon Choi, Li-Chiang Lin, and Jeffrey C. Grossman. Role of Structural Defects in the Water Adsorption Properties of MOF-801. *The Journal of Physical Chemistry C*, 122(10):5545–5552, March 2018. ISSN 1932-7447, 1932-7455. doi: 10.1021/acs. jpcc.8b00014.

[27] M. Vandichel, J. Hajek, A. Ghysels, A. De Vos, M. Waroquier, and V. Van Speybroeck. Water coordination and dehydration processes in defective UiO-66 type metal organic frameworks. *CrystEngComm*, 18(37):7056–7069, 2016. ISSN 1466-8033. doi: 10.1039/C6CE01027J.

A. Common characterisation techniques

A.1. Thermogravimetry

Thermogravimetry (TGA) is a standard laboratory technique where the weight of a sample is monitored while ambient temperature is controlled. Changes in sample mass can be correlated to physical events, such as adsorption, desorption, sample decomposition or oxidation, depending on temperature and its rate of change.

TGA experiments are carried out on approximately $15\,mg$ of sample with a TA Instruments Q500 up to $800\,°C$. The sample is placed on a platinum crucible and sealed in a temperature controlled oven, under gas flow of $40\,cm^3\,min^{-1}$. Experiments can use a blanket of either air or argon. The temperature ramp can be specified directly and should be chosen to ensure that the sample is in equilibrium with the oven temperature and no thermal conductivity effects come into play. Alternatively, a dynamic "Hi-Res" mode can be used which allows for automatic cessation of heating rate while the sample undergoes mass loss.

The main purpose of thermogravimetry as used in this thesis is the determination of sample decomposition temperature, to ensure that thermal activation prior to adsorption is complete and that all guest molecules have been removed without loss of structure. To this end, experiments are performed under an inert atmosphere (argon), and the sample activation temperature is chosen as $50\,°C$ to $100\,°C$ lower than the sample decomposition temperature.

A.2. Bulk density determination

Bulk density is a useful metric for the industrial use of adsorbent materials, as their volume plays a critical role in equipment sizing.

Bulk density is determined by weighing $1.5\,ml$ empty glass vessels and settling the MOFs inside. Powder materials are then added in small increments and settled through vibration between each addition. The full vessel is finally weighed, which allowed the bulk density to be determined. The same cell is used in all experiments, with cleaning through sonication between each experiment.

A.3. Skeletal density determination

True density or skeletal density is determined through gas pycnometry in a Microtrac-BEL BELSORP-max apparatus. Helium is chosen as the fluid of choice as it is assumed to be non-adsorbing.

The volume of a glass sample cell (V_c) is precisely measured through dosing of the reference volume with helium up to (p_1), then opening the valve connecting the two and allowing the gas to expand up to (p_2). Afterwards approximately 50 mg of sample are weighed and inserted in a glass sample cell. After sample activation using the supplied electric heater to ensure no solvent residue is left in the pores, the same procedure is repeated to determine the volume of the cell and the adsorbent. With the volume of the sample determined, the density can be calculated by.

$$V_s = V_c + \frac{V_r}{1 - \frac{p_1}{p_2}} \tag{A.1}$$

A.4. Nitrogen physisorption at $77\,\mathrm{K}$

Nitrogen adsorption experiments are carried out on a Micromeritics Triflex apparatus. Approximately 60 mg of sample are used for each measurement. Empty glass cells are weighed and filled with the samples, which are then activated in a Micromeritics Smart VacPrep up to their respective activation temperature under vaccum and then back-filled with an inert atmosphere. After sample activation, the cells are re-weighed to determine the precise sample mass. The cells are covered with a porous mantle which allows for a constant temperature gradient during measurement by wicking liquid nitrogen around the cell. Finally, the cells are immersed in a liquid nitrogen bath and the adsorption isotherm is recoded using the volumetric method. A separate cell is used to condense the adsorptive throughout the measurement for accurate determination of its saturation pressure.

A.5. Vapour physisorption at $298\,\mathrm{K}$

Vapour adsorption isotherms throughout this work are measured using a MicrotracBEL BELSORP-max apparatus in vapour mode. Glass cells are first weighed and then filled with about 50 mg of sample. The vials are then heated under vacuum up to the activation temperature of the material and re-weighed in order to measure the exact sample mass without adsorbed guests. The cells are then immersed in a mineral oil bath kept at 298 K. To ensure that the cold point of the system occurs in the material and to prevent condensation on cell walls, the reference volume, dead space and vapour source are temperature controlled through an insulated enclosure.

A.6. Gravimetric isotherms

The gravimetric isotherms in this thesis are obtained using a commercial Rubotherm GmbH balance. Approximately 1 g of dried sample is used for these experiments. Samples are activated in situ by heating under vacuum. The gas is introduced using a step-by-step method, and equilibrium is assumed to have been reached when the variation of weight remained below 30 µg over a 15 min interval. The volume of the sample is determined from a blank experiment with helium as the non-adsorbing gas and used in combination with the gas density measured by the Rubotherm balance to compensate for buoyancy.

A.7. High throughput isotherm measuremnt

A high-throughput gas adsorption apparatus is presented for the evaluation of adsorbents of interest in gas storage and separation applications. This instrument is capable of measuring complete adsorption isotherms up to 50 bar on six samples in parallel using as little as 60 mg of material. Multiple adsorption cycles can be carried out and four gases can be used sequentially, giving as many as 24 adsorption isotherms in 24 h.[1]

A.8. Powder X-ray diffraction

A.9. Nuclear magnetic resonance

Bibliography

[1] Andrew D. Wiersum, Christophe Giovannangeli, Dominique Vincent, Emily Bloch, Helge Reinsch, Norbert Stock, Ji Sun Lee, Jong-San Chang, and Philip L. Llewellyn. Experimental Screening of Porous Materials for High Pressure Gas Adsorption and Evaluation in Gas Separations: Application to MOFs (MIL-100 and CAU-10). *ACS Combinatorial Science*, 15(2):111–119, February 2013. ISSN 2156-8952. doi: 10. 1021/co300128w.

B. Synthesis method of referenced materials

B.1. Takeda 5A reference carbon

The Takeda 5A carbon was purchased directly from the Takeda corporation. The sample was activated at 250 °C under secondary vacuum (5 mbar) before any measurements.

full char- acteri- zation

B.2. MCM-41 controlled pore glass

MCM-41 (Mobil Composition of Matter No. 41) is a mesoporous silica (SiO_2) material with a narrow pore distribution. First synthesised by the Mobil Oil Corporation, it is produced through templated synthesis using mycelle-forming surfactants. The material referenced in this thesis was purchased from Sigma-Aldrich. The activation procedure consists of heating at 250 °C under secondary vacuum (5 mbar).

B.3. Zr fumarate MOF

The synthesis of the Zr fumarate was performed in Peter Behren's group in Hannover, through modulated synthesis. This MOF can only be synthesised through the addition of a modulator, in this case fumaric acid, to the ongoing reactor, as detailed in the original pubication.[1]

The procedure goes as follows: $ZrCl_4$ (0.517 mmol, 1 eq) and fumaric acid (1.550 mmol, 3 eq) are dissolved in 20 mL N,N-dimethylformamide (DMF) and placed in a 100 mL glass flask at room temperature. 20 equivalents of formic acid were added. The glass flasks were Teflon-capped and heated in an oven at 120 °C for 24 h. After cooling, the white precipitate was washed with 10 mL DMF and 10 mL ethanol, respectively. The washing process was carried out by centrifugation and redispersion of the white powder, which was then dried at room temperature over night

B.4. UiO-66(Zr) for defect study

The UiO-66(Zr) sample preparation was adapted from Shearer et al. [2] as follows: $ZrCl_4$ (1.55 g, 6.65 mmol), an excess of terephthalic acid (BDC) (1.68 g, 10.11 mmol), HCl 37 % solution (0.2 mL, 3.25 mmol) and N,N'-dimethylformamide (DMF) (200 mL,

2.58 mol) were added to a 250 mL pressure resistant Schott bottle. The mixture was stirred for 10 min, followed by incubation in a convection oven at 130 °C for 24 h. The resulting white precipitate was washed with fresh DMF (3× 50 mL) followed by ethanol (3× 50 mL) over the course of 48 h and dried at 60 °C. After drying, the sample was activated on a vacuum oven by heating at 200 °C under vacuum for 12 h. The yield was 78 % white microcrystalline powder. Before the experiment, the sample was calcined at 200 °C under vacuum (5 mbar) to remove any residual solvents from the framework.

B.5. UiO-66(Zr) for shaping study

The scaled-up synthesis of UiO-66(Zr) was carried out in a 5 L glass reactor (Reactor Master, Syrris, equipped with a reflux condenser and a Teflon-lined mechanical stirrer) according to a previously reported method.[3] In short, 462 g (2.8 mol) of H_2BDC (98%) was initially dissolved in 2.5 L of dimethyl formamide (DMF, 2.36 kg, 32.3 mol) at room temperature. Then, 896 g (2.8 mol) of $ZrOCl_2 \cdot 8H_2O$ (98%) and 465 mL of 37% HCl (548 g, 15 mol) were added to the mixture. The molar ratio of the final $ZrOCl_2 \cdot 8H_2O/H_2BDC/DMF/HCl$ mixture was 1 : 1 : 11.6 : 5.4. The reaction mixture was vigorously stirred to obtain a homogeneous gel. The mixture was then heated to 423 K at a rate of $1 \, \text{K} \, \text{min}^{-1}$ and maintained at this temperature for 6 h in the reactor without stirring, leading to a crystalline UiO-66(Zr) solid. The resulting product (510 g) was recovered from the slurry by filtration, redispersed in 7 L of DMF at 333 K for 6 h under stirring, and recovered by filtration. The same procedure was repeated twice, using methanol (MeOH) instead of DMF. The solid product was finally dried at 373 K overnight.

B.6. MIL-100(Fe) for shaping study

The synthesis of the MOF for the shaping study was done at the KRICT institute using a previously published method.[4] To synthesise the MIL-100(Fe) material $Fe(NO_3)_3$ was completely dissolved in water. Then, trimesic acid (BTC) was added to the solution; the resulting mixture was stirred at room temperature for 1h. The final composition was $Fe(NO_3)_3 \cdot 9H_2O$:0.67 BTC:n H_2O (x= 55–280). The reactant mixture was heated at 433 K for 12 h using a Teflon-lined pressure vessel. The synthesized solid was filtered and washed with deionized (DI) water. Further washing was carried out with DI water and ethanol at 343 K for 3 h and purified with a 38 mM NH_4F solution at 343 K for 3 h. The solid was finally dried overnight at less than 373 K in air.

B.7. MIL-127(Fe) for shaping study

MIL-127(Fe) was synthesized by reaction of $Fe(ClO_4)_3 \cdot 6H_2O$ (3.27 g, 9.2 mmol) and $C_{16}N_2O_8H_6$ (3.3 g) in DMF (415 mL) and hydrofluoric acid (5 M, 2.7 mL) at 423 K in a Teflon flask. The obtained orange crystals were placed in DMF (100 mL) and

stirred at ambient temperature for 5 h. The final product was kept at 375 K overnight. MIL-127(Fe) was synthesized by reaction of $Fe(ClO_4)_3 \cdot 6 H_2O$ (3.27 g, 9.2 mmol) and $C_{16}N_2O_8H_6$ (3.3 g) in DMF (415 mL) and hydrofluoric acid (5 M, 2.7 mL) at 423 K in a Teflon flask. The obtained orange crystals were placed in DMF (100 mL) and stirred at ambient temperature for 5 h. The final product was kept at 375 K overnight.

Bibliography

[1] Gesa Wißmann, Andreas Schaate, Sebastian Lilienthal, Imke Bremer, Andreas M. Schneider, and Peter Behrens. Modulated synthesis of Zr-fumarate MOF. *Microporous and Mesoporous Materials*, 152:64–70, April 2012. ISSN 13871811. doi: 10.1016/j.micromeso.2011.12.010.

[2] Greig C. Shearer, Sachin Chavan, Jayashree Ethiraj, Jenny G. Vitillo, Stian Svelle, Unni Olsbye, Carlo Lamberti, Silvia Bordiga, and Karl Petter Lillerud. Tuned to Perfection: Ironing Out the Defects in Metal–Organic Framework UiO-66. *Chemistry of Materials*, 26(14):4068–4071, July 2014. ISSN 0897-4756, 1520-5002. doi: 10.1021/cm501859p.

[3] Florence Ragon, Patricia Horcajada, Hubert Chevreau, Young Kyu Hwang, U-Hwang Lee, Stuart R. Miller, Thomas Devic, Jong-San Chang, and Christian Serre. In Situ Energy-Dispersive X-ray Diffraction for the Synthesis Optimization and Scale-up of the Porous Zirconium Terephthalate UiO-66. *Inorganic Chemistry*, 53(5):2491–2500, March 2014. ISSN 0020-1669, 1520-510X. doi: 10.1021/ic402514n.

[4] Felix Jeremias, Stefan K. Henninger, and Christoph Janiak. Ambient pressure synthesis of MIL-100(Fe) MOF from homogeneous solution using a redox pathway. *Dalton Transactions*, 45(20):8637–8644, 2016. ISSN 1477-9226, 1477-9234. doi: 10.1039/C6DT01179A.